J. Ind. Eng. Chem., **Vol. 13**, No. 7, (2007) 1174-1179

Improved High-rate Capability of $Li[Ni_{0.5}Co_yMn_{1.5-y}]O_{4-z}F_z$ Spinel Materials for 5 V Lithium Secondary Batteries

Sung Woo Oh, Sang-Ho Park*, E. Jung, Young Chan Bae, and Yang-Kook Sun †**

Department of Chemical Engineering, Center for Information and Communication Materials, Hanyang University, Seoul 133-791, Korea
**Argonne National Laboratory, 9700 S. Cass Ave, Argonne, IL 60439, U.S.A.*
***Department of Digital Culture & Contents, Dong-Eui University, Busan 614-714, Korea*

Received September 18, 2007; Accepted December 14, 2007

Abstract: The effects of substituting cobalt and fluorine for manganese and oxygen on the structural and electrochemical properties of $Li[Ni_{0.5}Co_yMn_{1.5-y}]O_{4-z}F_z$ cathode materials were studied. The pure phase $Li[Ni_{0.5}Co_yMn_{1.5-y}]O_{4-z}F_z$ ($y = 0$ - 1.0, $z = 0$ - 0.1) spinel materials were successfully synthesized at 900 °C by an ultrasonic spray pyrolysis method. The $Li[Ni_{0.5}Co_yMn_{1.5-y}]O_{4-z}F_z$ ($y = 0$ - 1.0, $z = 0$ - 0.1) powders were characterized by means of X-ray diffraction (XRD), Rietveld refinements, scanning electron microscopy (SEM), energy dispersive spectra (EDS), Brunauer-Emmett-Teller (BET) analysis, and galvanostatic charge/discharge testing. The cobalt and fluorine substitutions were effective for improving the high current discharge capability, even though the electrode was cycled with a discharge current density of 1,350 mA g^{-1} (10 C-rate).

Keywords: *high rate property, 5 V spinel, fluorine doping, cobalt doping, cathode materials*

Introduction

Spinel lithium manganese oxide, $Li_xMn_2O_4$, and its derivatives are considered to be promising for use as cathode materials for rechargeable lithium batteries because of their advantages, which include low cost, non-toxicity, abundance, and relatively high specific energy [1-4]. However, the Jahn-Teller effect involving Mn^{3+} ions induces a structural instability due to anisotropic volume changes through a cubic-tetragonal transition, which leads to a loss of electrode performance in extended battery cycling [5].

One possible approach for improving the cycling performance of $LiMn_2O_4$ is the partial substitution of manganese with other transition metals such as Cr, Co, Fe, and Ni [6-8]. The capacity and voltage plateau in $Li/LiM_xMn_{2-x}O_4$ cells strongly depend on the type and content of the transition metal (M). Among those materials, $LiNi_{0.5}Mn_{1.5}O_4$ has received much attention for its dominant potential plateau at 4.7 V, while other materials exhibited two plateaus around 4 and 5 V. However, defect are commonly found in the preparation of solid $LiNi_{0.5}Mn_{1.5}O_4$ materials, and $Li_xNi_{1-x}O_4$ impurities have been identified that cause a decrease in the 5 V gravimetric capacity [6]. Moreover, the resulting Ni deficiency in the spinel phase involves the presence of Mn^{3+}, which leads to a significant extension of the 4 V plateau at the expense of the nominal 142 mAhg^{-1} capacity at 5 V. Recently, to improve the cycle performance in the 5 V range, several research groups have investigated the properties of $LiNi_yCo_{1-2y}Mn_{1+y}O_4$ [9] and $Li[Ni_{(0.5+x)}Mn_{(1.5-2x)}Mo_x]O_4$ [10]. Recently, our group determined that anion substitution in the form of spinel oxyfluorides improves the storage performance of spinel cathode materials [11].

In this work, we attempted to synthesize cation (Co^{3+}) and anion (F^{-1}) doped $Li[Ni_{0.5}Co_yMn_{1.5-y}]O_{4-z}F_z$ ($y = 0$ - 1.0, $z = 0$ - 0.1) materials. A nominal charge balance of these materials is $Li[Ni_{0.5}{}^{2+}Co_y{}^{3+}Mn_{1.5-y}{}^{4+}]O^{-2}{}_{4-z}F^{-1}{}_z$. The structural and electrochemical properties of the prepared materials were characterized by XRD and electrochemical testing, respectively. This work represents the first reported cation and anion co-doped 5 V spinel

† To whom all correspondence should be addressed.
(e-mail: yksun@hanyang.ac.kr)

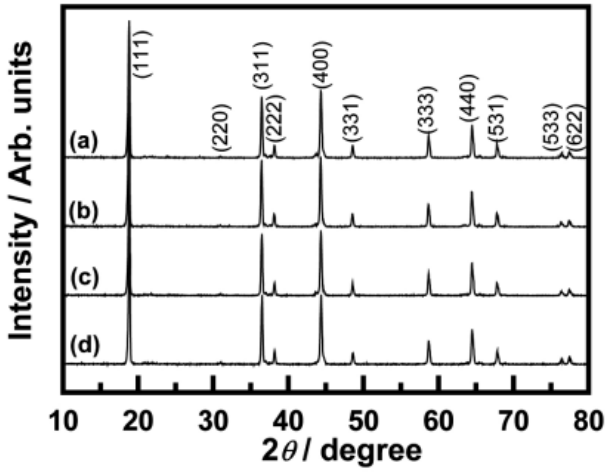

Figure 1. X-ray diffraction patterns of $Li[Ni_{0.5}Co_yMn_{1.5-y}]O_{4-z}F_z$ powders: (a) $Li[Ni_{0.5}Mn_{1.5}]O_4$, (b) $Li[Ni_{0.5}Co_{0.05}Mn_{1.45}]O_4$, (c) $Li[Ni_{0.5}Co_{0.05}Mn_{1.45}]O_{3.95}F_{0.05}$, and (d) $Li[Ni_{0.5}Co_{0.1}Mn_{1.4}]O_{3.9}F_{0.1}$.

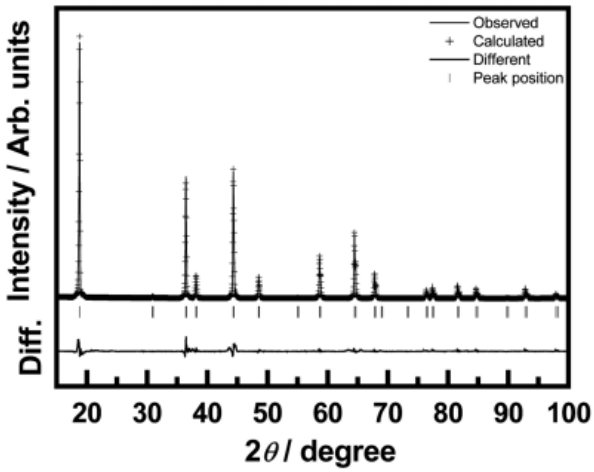

Figure 2. X-ray Rietveld refined pattern of $Li[Ni_{0.5}Co_{0.05}Mn_{1.45}]O_4$ material.

$Li[Ni_{0.5}Co_yMn_{1.5-y}]O_{4-z}F_z$ (y = 0 - 1.0, z = 0 - 0.1) cathode materials prepared by an ultrasonic spray pyrolysis method.

Experimental

$Li[Ni_{0.5}Co_yMn_{1.5-y}]O_{4-z}F_z$ (y = 0 - 1.0, z = 0 - 0.1) powders were prepared by an ultrasonic spray pyrolysis method. Stoichiometric amounts of nickel nitrate hexahydrate ($Ni(NO_3)\cdot 6H_2O$, Aldrich), cobalt nitrate hexahydrate ($Co(NO_3)_2\cdot 6H_2O$, Aldrich), and manganese nitrate tetrahydrate ($Mn(NO_3)_2\cdot 4H_2O$, Sigma) salts were dissolved in distilled water. The dissolved solution was added into a continuously agitated aqueous citric acid solution. The molar concentration of citric acid was fixed at 0.2 M and NH_4OH was added to the starting solution in order to maintain a solution pH of 7. Atomization of the starting solution was performed using an ultrasonic nebulizer with a resonant frequency of 1.7 MHz. The resulting aerosol stream was introduced into a vertical quartz reactor (heated to 500 ^oC) with an inner diameter and length of 50 and 1200 mm, respectively. Air was used as a carrier gas and a flow rate of 10 L min^{-1} was maintained. The precursor powders obtained were mixed with excess amounts of $LiOH\cdot H_2O$ and LiF. The mixture was then softly ground and heated to 900 ^oC at a heating rate of 1 ^oC min^{-1}. A powder X-ray diffraction (XRD, Rint-2000, Rigaku, Japan) measurement using Cu-Kα radiation was employed to identify the crystalline phase of the synthesized material. Rietveld refinement of the collected data was made using the FULLPROF Rietveld program [12]. Particle morphology and nominal elemental compositions of the powders were observed using a scanning electron microscope and energy dispersive spectra (SEM, EDS, JSM 6400, JEOL, Japan), respectively. Galvanostatic charge/discharge cycling was performed using a 2032-type coin cell. Cathodes were prepared by blending $Li[Ni_{0.5}Co_yMn_{1.5-y}]O_{4-z}F_z$, Super P carbon black, and polyvinylidene fluoride (PVDF) (80:10:10) in N-methyl-2-pyrrolidone (NMP). The slurry was then cast on aluminum foil and dried at 110 ^oC overnight under vacuum. Disks were then punched out of the foil. Lithium foil (Cyprus Foote Mineral Co.) was used as the anode. The electrolyte solution used was 1 M $LiPF_6$ in a mixture of ethylene carbonate (EC) and diethyl carbonate (DEC) in a 1:1 volume ratio (Cheil Industries Inc. Korea). The charge/discharge measurements were carried out between 3.5 and 5 V (vs. Li/Li^+) with a current density of 27 mA g^{-1} (0.2 C-rate) at room temperature (30 ^oC).

Results and Discussion

$Li[Ni_{0.5}Co_yMn_{1.5-y}]O_{4-z}F_z$ powders were synthesized within the ranges of y = 0 - 1.0 and z = 0 - 0.1 by an ultrasonic spray pyrolysis method. Figure 1 shows X-ray diffraction patterns of solids prepared with various cobalt and fluorine content as described in the $Li[Ni_{0.5}Co_yMn_{1.5-y}]O_{4-z}F_z$ formula. The Rietveld refinement analysis of the selected $Li[Ni_{0.5}Co_{0.05}Mn_{1.45}]O_4$ materials is shown in Figure 2. The structure of $Li[NI_{0.5}Co_{0.05}Mn_{1.5}]O_4$ was refined in the space group Fd_3m in the well-known spinel type with basic crystallographic positions. For Li^+ ions, the crystallographic positions were 8a [1/8,1/8,1/8] with local symmetry. For Ni^{2+}, Co^{3+}, and $Mn^{3+/4+}$ ions, the crystallographic positions were at the 16d [1/2,1/2,1/2] site. Also, oxygen was in the 32e [u,u,u] (u in 0.2623(8)) positions. There is a possibility that small amounts of transition metal ions may also occupy the 8a site. All transition metal scattering

Table 1. The Variation of Lattice Constants, a_h, Volume, Specific Surface Area (S_a), and Summary of High Current Capabilities of the $Li[Ni_{0.5}Co_yMn_{1.5-y}]O_{4-z}F_z$ Materials

Initial composition	a_h (Å)	Volume (Å^3)	S_a (m^2/g)	Current density		Retention (%)
				135 mA g^{-1} (1 C-rate)	1,350 mA g^{-1} (10 C-rate)	
y = 0, z = 0	8.179 (5)	547.24 (3)	3.79	135 mA g^{-1}	47 mA g^{-1}	35
y = 0.05, z = 0	8.172 (9)	546.75 (9)	0.66	120 mA g^{-1}	52 mA g^{-1}	44
y = 0.05, z = 0.05	8.171 (9)	545.71 (1)	0.86	110 mA g^{-1}	79 mA g^{-1}	71
y = 0.1, z = 0.1	8.169 (1)	545.16 (0)	1.25	106 mA g^{-1}	86 mA g^{-1}	81

factors are very close to each other and it is therefore hard to confirm a difference between these three ions in specific crystallographic positions. However, due to the large difference in scattering factors between Li and transition metal ions, it was possible to refine the small occupancy of transition metals in the 8a site with relatively high accuracy due to the smaller difference between both intensities and the Bragg R-factor of 6.98 %. Therefore, the refinement pattern could be identified as a cubic spinel structure with a space group, Fd_3m Also, the observed diffraction lines show that the intensity ratio of the I (111) and I (311) directions are larger than the unit and the negligible peak of the I (220) direction; these observations agree well with a distribution of cations. Therefore, we can assume that the lithium ions occupy the tetrahedral (8a) sites, Ni^{2+}, Co^{3+}, and $Mn^{3+/4+}$ ions are located at the octahedral (16d) sites, and O^{2-} ions are located at the (32e) sites.

The calculated lattice constants, a_h, of the cubic spinel unit cell of the samples with varying cobalt and fluorine content are shown in Table 1. As the cobalt and fluorine contents were increased, a_h decreased from 8.179(5) to 8.169(1) Å. The lattice constant decreased with an increase in the amount of cobalt, which is related to the smaller ionic radius of cobalt (0.61 Å for high spin Co^{3+} and 0.645 Å for high spin Mn^{3+}). The decrease in the lattice constant is also due to the substitution of manganese by cobalt at the 16d sites as well as the higher Co-O (1,067 kJ mol^{-1}) bond strength compared to that of Mn-O (946 kJ mol^{-1}) [13]. G.T.-K. Fey and coworkers reported that with Al-substituted systems, a deviation from Vegard's law was observed [14]. In this case, the deviation from Vegard's law may have been related to the presence of extraneous phases, especially those with higher concentrations of Al. These parameter values and their decrease with increasing cobalt content are in agreement with results reported in the literature for lithium-cobalt-manganese compounds [13]. Moreover, fluorine ions also cause a decrease in the lattice parameter because of the 16d site of manganese and the strong bond energy of Li-F.

Scanning electron microscopy (SEM) images for the post-calcined $Li[Ni_{0.5}Co_yMn_{1.5-y}]O_{4-z}F_z$ (y = 0 - 1.0, z = 0 - 0.1) powders are shown in Figure 3. Morphological changes are clearly seen as a result of cobalt and fluorine substitution. In our previous work [15], $Li[Ni_{0.5}Mn_{1.5}]O_4$ spinel powders showed a well-developed octahedron morphological shape, as shown in Figure 3(a). When cobalt was substituted for manganese, $Li[Ni_{0.5}Co_{0.05}Mn_{1.45}]O_4$ particles are less defined and smaller particles are observed. Furthermore, an aggregation effect causes a complicated texture based on dendrite agglomerates of particles [9]. However, as fluorine ions are substituted by adding with LiF, the particles became larger and had a narrower size distribution than that of the unsubstituted samples as shown in Figure 3(b). A similar phenomenon was also reported with fluorine substituted in $Li[Ni_{0.5}Mn_{1.5}]O_{4-y}F_y$ [11]. In this case, the introduction of a small amount of fluorine led to the development of larger, square-shaped particles. J. R. Dahn and coworkers reported that the LiF additives are able to act on sintering agents, which can increase the tapping density of materials [16]. The specific surface areas for all the samples were measured by the BET method and are listed in Table 1. By introducing Co and/or F ions, the specific surface areas decreased slightly. In order to confirm the

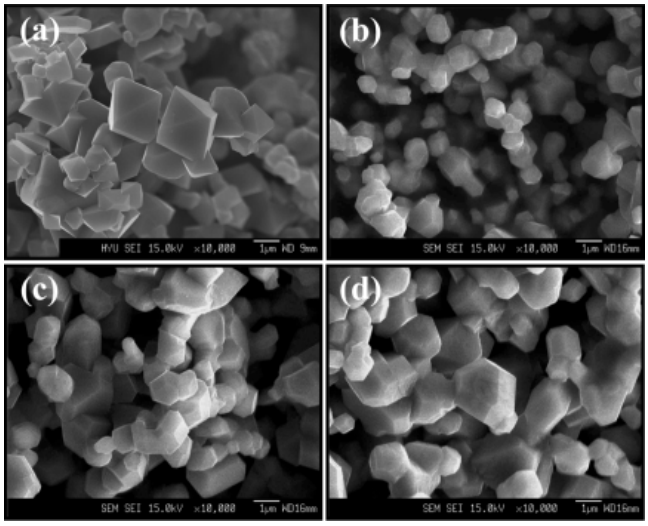

Figure 3. SEM images of $Li[Ni_{0.5}Co_yMn_{1.5-y}]O_{4-z}F_z$ powders: (a) $Li[Ni_{0.5}Mn_{1.5}]O_4$, (b) $Li[Ni_{0.5}Co_{0.05}Mn_{1.45}]O_4$, (c) $Li[Ni_{0.5}Co_{0.05}Mn_{1.45}]O_{3.95}F_{0.05}$, and (d) $Li[Ni_{0.5}Co_{0.1}Mn_{1.4}]O_{3.9}F_{0.1}$.

Table 2. Energy Dispersive Spectra (EDS) Analysis Data for $Li[Ni_{0.5}Co_{0.1}Mn_{1.4}]O_{4-z}F_z$ Materials with an Initial z Content of 0.1

Element	App. Conc.	K ratio	Intensity	App. Weight %
Pt	2.88	0.0287 (7)	0.7027	4.61
Ni	11.28	0.1188 (0)	0.9127	14.67
Co	2.99	0.0299 (4)	0.8749	3.86
Mn	37.42	0.3741 (7)	0.9359	45.06
F	0.51	0.0039 (1)	0.2181	2.63
O	46.05	0.1787 (4)	1.7794	29.17

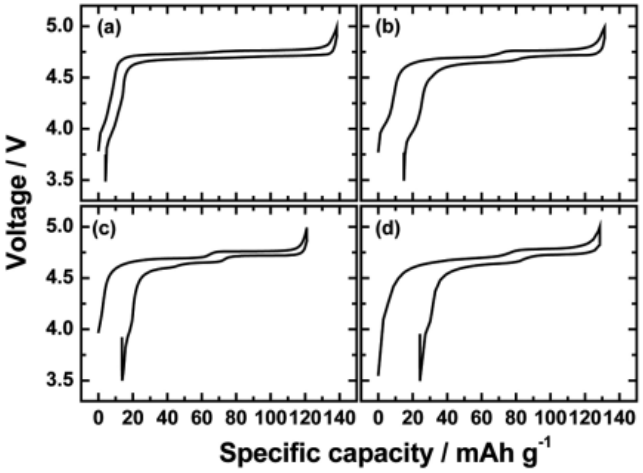

Figure 4. Voltage profile vs. specific capacity of $Li/Li[Ni_{0.5}Co_yMn_{1.5-y}]O_{4-z}F_z$ cells cycled between 3.5 and 5.0 V at a constant current density of 27 mA g^{-1}: (a) $Li[Ni_{0.5}Mn_{1.5}]O_4$, (b) $Li[Ni_{0.5}Co_{0.05}Mn_{1.45}]O_4$, (c) $Li[Ni_{0.5}Co_{0.05}Mn_{1.45}]O_{3.95}F_{0.05}$, and (d) $Li[Ni_{0.5}Co_{0.1}Mn_{1.4}]O_{3.9}F_{0.1}$.

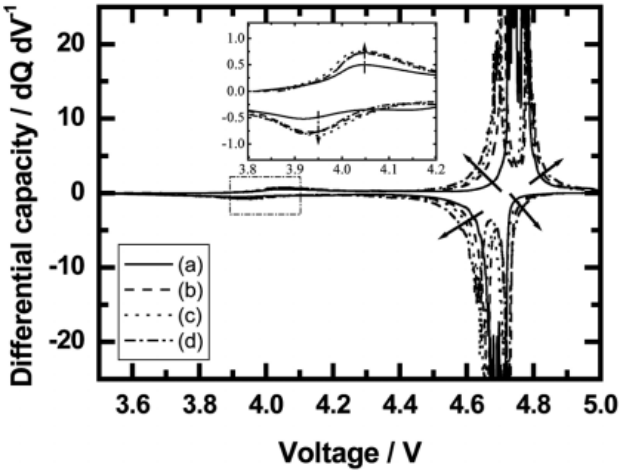

Figure 5. Differential capacity vs. voltage curves for $Li/Li[Ni_{0.5}Co_yMn_{1.5-y}]O_{4-z}F_z$ cells: (a) $Li[Ni_{0.5}Mn_{1.5}]O_4$, (b) $Li[Ni_{0.5}Co_{0.05}Mn_{1.45}]O_4$, (c) $Li[Ni_{0.5}Co_{0.05}Mn_{1.45}]O_{3.95}F_{0.05}$, and (d) $Li[Ni_{0.5}Co_{0.1}Mn_{1.4}]O_{3.9}F_{0.1}$.

nominal compositions, an Energy Dispersive Spectra (EDS) analysis was performed and the results are shown in Table 2. EDS results confirmed the nominal elemental compositions of each transition metal as well as that of O and F.

In our recent results for F^{-1} substituted on Ni-Co-Mn layered materials, fluorine ions successfully substituted for oxygen sites, more closed at the surface, followed by possible changes in the oxidation state of the transition metal ions as confirmed by XPS analysis [17,18]. More recently, Manthiram's group also reported that an oxyfluoride spinel, such as $LiMn_{1.8}Li_{0.1}Ni_{0.1}O_{3.8}F_{0.2}$, exhibited superior cycling properties compared to normal $LiMn_2O_4$ materials [19]. Their results were thought to have originated from significantly suppressed manganese dissolution. We did not address the exact content and distribution of F^{-1} ions in this study. Thus, we will report the electronic and local structures of the delithiated-relithiated $Li[Ni_{0.5}Co_yMn_{1.5-y}]O_{4-z}F_z$ system, *in situ* transition metal K-edge X-ray absorption spectroscopic (XAS), and IC in the near future.

Figure 4 shows the voltage profiles vs. specific capacity of the $Li/Li[Ni_{0.5}Co_yMn_{1.5-y}]O_{4-z}F_z$ cells during galvanostatic charge/discharge cycling. The $Li/Li[Ni_{0.5}Co_yMn_{1.5-y}]O_{4-z}F_z$ cells were cycled between 3.5 and 5 V with a constant current density of 27 mA g^{-1} (0.2 C-rate). The flat voltage profiles observed around the 4.7 and 4.1 V regions are attributed to the $Ni^{2+/4+}$ and $Mn^{3+/4+}$ redox reactions, respectively [6,8,10,20]. However, as the cobalt and fluorine doping contents were increased, $Li/Li[Ni_{0.5}Co_yMn_{1.5-y}]O_{4-z}F_z$ cells showed steeper voltage profiles, which are attributed to $Co^{3+/4+}$ redox reactions and to Co^{3+} ions reducing some of the Mn^{4+} to an oxidation state of Mn^{3+}. Recently, R. M. Sojas and coworkers. reported that their cobalt-doped spinel had the same $Co^{3+/4+}$ redox couples as compared to $Ni^{2+/4+}$ redox potentials, so that $Co^{3+/4+}$ redox reactions were detected as overlapping around the 4.7 V region [20]. Moreover, B. J. Hwang and coworkers [21] and J.-H. Kim and coworkers [22] observed similar phenomena, in spite of the absence of Co ions. Therefore, a more detailed study on the electronic state and the local structures of the delithiated-relithiated $Li[Ni_{0.5}Co_yMn_{1.5-y}]O_{4-z}F_z$ system should be undertaken.

Figure 5 shows differential capacities vs. voltage curves at the 1st cycle for the $Li/Li[Ni_{0.5}Co_yMn_{1.5-y}]O_{4-z}F_z$ cells. All cells showed two redox peaks at around

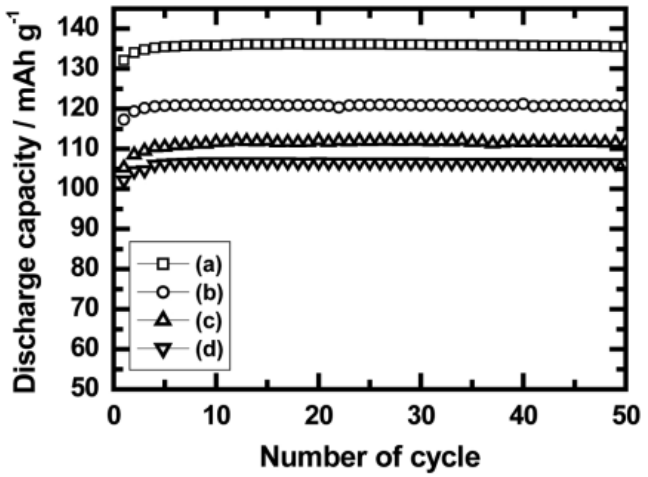

Figure 6. Discharge capacity vs. number of cycles for Li/Li$[Ni_{0.5}Co_yMn_{1.5-y}]O_{4-z}F_z$ cells cycled between 3.5 and 5.0 V at a constant current density of 27 mA g^{-1}: (a) $Li[Ni_{0.5}Mn_{1.5}]O_4$, (b) $Li[Ni_{0.5}Co_{0.05}Mn_{1.45}]O_4$, (c) $Li[Ni_{0.5}Co_{0.05}Mn_{1.45}]O_{3.95}F_{0.05}$, and (d) $Li[Ni_{0.5}Co_{0.1}Mn_{1.4}]O_{3.9}F_{0.1}$.

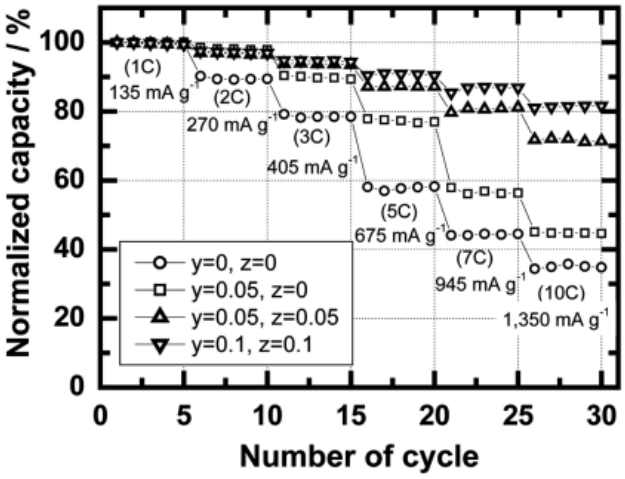

Figure 7. Normalized capacity vs. number of cycles for Li/ Li$[Ni_{0.5}Co_yMn_{1.5-y}]O_{4-z}F_z$ cells with various current densities between 3.5 and 5.0 V. The cells were charged using a current density of 27 mA g^{-1} (0.2 C-rate).

the 4.7 and 4.1 V regions during the oxidation-reduction process, which are attributed to the $Ni^{2+/4+}$ and $Mn^{3+/4+}$ redox reactions, respectively [10]. As the cobalt and fluorine content increased, $Ni^{2+/4+}$ and $Mn^{3+/4+}$ redox peaks resulted in broadening of the 4.7 and 4.0 V regions, respectively; this result may be caused by participating $Co^{3+/4+}$ ions. As the Co doping content increased, the discharge capacities also decreased. This observation of the decrease in the electrochemical capacities is in agreement with a previous report [23].

Figure 6 shows the cycling performances of the Li/Li$[Ni_{0.5}Co_yMn_{1.5-y}]O_{4-z}F_z$ (y = 0 - 1.0, z = 0 - 0.1) cells. As the cobalt doping content increased, Li/Li $[Ni_{0.5}Co_yMn_{1.5-y}]O_{4-z}F_z$ cells exhibited lower discharge capacities than that of the Li/$Li[Ni_{0.5}Mn_{1.5}]O_4$ cell, which can be attributed to a shift to higher voltage regions and broadening of the redox peaks in the 4.7 V region. Moreover, the introduction of fluorine ions resulted in a decrease in discharge capacity because F^{-1} ions replaced O^{2-} ions. The stronger bond energy of Li-F (557 KJ mol^{-1}) compared with that of Li-O (333 KJ mol^{-1}) resulted in more energy to the (de)intercalation of lithium ions. However, all Li/Li$[Ni_{0.5}Co_yMn_{1.5-y}]O_{4-z}F_z$ (y = 0 - 1.0, z = 0 - 0.1) cells had cycling performances of almost 100 %, even after the 50th cycle, indicating that high purity materials can be obtained using ultrasonic spray pyrolysis.

Figure 7 shows the various applied discharge current densities for Li/Li$[Ni_{0.5}Co_yMn_{1.5-y}]O_{4-z}F_z$ (y = 0 - 1.0, z = 0 - 0.1) cells with potential limits of 3.5～5.0 V. The cells were charged using a constant current density of 27 mA g^{-1} (0.2 C-rate) before each discharge test. The capacity difference between the electrodes became larger as the applied current density increased. The Li$[Ni_{0.5}Mn_{1.5}]O_4$ electrode discharge capacity decreased very rapidly with increasing current density. However, $Li[Ni_{0.5}Co_{0.05}Mn_{1.45}]O_{3.95}F_{0.05}$ and $Li[Ni_{0.5}Co_{0.1}Mn_{1.4}]O_{3.9}F_{0.1}$ electrodes delivered a normalized discharge capacity of 70 and 80 % at 1350 mA g^{-1} (10 C-rate), respectively, compared to the 135 mA g^{-1} (1C-rate) current density. Li^+ ions diffuse through the electrolyte and solid-state lithium ions diffuse within the electrode. The high current capability is related to a combination of electrode polarization and electric conductivity of the host material. In fact, the electric conductivity of Co is greater than that of Mn, and a small amount of cobalt doping increases electric conductivity. Moreover, the observed reductions of the spinel lattice and cell volume with cobalt doping arise from a local contraction of the manganese lattice about the substituted Co^{3+} ions [13]. Therefore, electrochemical insertion/extraction of lithium ions was more easily performed with Li$[Ni_{0.5}Co_yMn_{1.5-y}]O_{4-z}F_z$ than $Li[Ni_{0.5}Mn_{1.5}]O_4$. Moreover, Amatucci and coworkers [24] also reported that a small amount of F ions form Mn-F bonds, which may affect the chemical stability of the spinel towards Mn dissolution initiated by acidic species. Therefore, it seems that the small amount of Co and F substitution in the $Li[Ni_{0.5}Mn_{1.5}]O_4$ structure enhances the electrochemical performance resulting in a significant improvement in rate capability of $Li[Ni_{0.5}Mn_{1.5}]O_4$.

Conclusion

Spinel Li$[Ni_{0.5}Co_yMn_{1.5-y}]O_{4-z}F_z$ (y = 0 - 1.0, z = 0 - 0.1) materials were synthesized by an ultrasonic spray pyrolysis method. All materials had a cubic spinel structure with a space group of Fd_3m and high crystallinity with

well-developed morphology. Cobalt and fluorine co-doped materials exhibited lower discharge capacities than $Li[Ni_{0.5}Mn_{1.5}]O_4$. However, Co and F-doped spinel materials such as the $Li[Ni_{0.5}Co_{0.1}Mn_{1.4}]O_{3.9}F_{0.1}$ electrode showed a excellent high current discharge capability, 80 % higher, even when applied at 10 times the 135 mA g^{-1} (1 C-rate) current density. They also showed 100 % cycling retention after 50 cycles.

Acknowledgements

This research was supported by the University IT Research Center Project.

References

1. S. Megahed and B. Scrosati, *J. Power Sources*, **51**, 79 (1994).
2. J. M. Tarascon, E. Wang, F. K. Shokoohi, W. R. Mckinnon, and S. Colson, *J. Electrochem. Soc*., **138**, 2859 (1991).
3. C. W. Lee, *J. Ind. Eng. Chem*., **12**, 967 (2006).
4. H. Yang, S. Amiruddin, H. Bang, Y. Sun, and J. Prakash, *J. Ind. Eng. Chem.*, **12**, 12 (2006).
5. A. Yamada, M. Tanaka, and K. Sekai, *J. Power Sources*, **81**, 73 (1999).
6. Q. Zhong, A. Banakdarpour, M. Zhang, Y. Gao, and J. R. Dahn, *J. Electrochem. Soc*., **144**, 205 (1997).
7. S. Shigemura, S. Sakaebe, H. Kageyama, H. Kobayashi, A. R. West, R. Kanno, S. Morimoto, S. Nasu, and M. Tabuchi, *J. Electrochem. Soc*., **148**, A730 (2001).
8. K. Amine, H. Tukamoto, H. Yasuda, and Y. A. Fujita, *J. Electrochem. Soc*., **143**, 1607 (1996).
9. R. Alcantara, M. Jaraba, P. Lavela, and J. L. Tirado, *J. Electrochem. Soc*., **151**, A53 (2004).
10. S.-H. Park, S.-W. Oh, S.-T. Myung, and Y.-K. Sun, *Electrochem. and Solid-State Lett*., **7**, A451 (2004).
11. S.-W. Oh, S.-H. Park, J.-H. Kim, Y. C. Bae, and Y.-K. Sun, *J. Power Sources*, **157**, 464 (2006).
12. T. Roisnel and J. Rodriguez-Carjaval, Fullprof Manual, Institute Laue-Langevin, Grnoble (2000).
13. P. Aitchison, B. Ammundsen, D. J. Jones, G. Burns, and J. Roziere, *J. Mater. Chem*., **9**, 3125 (1999).
14. G. T.-K. Fey, C.-Z. Lu, and T. P. Kumar, *J. Power Sources*, **115**, 332 (1999).
15. S.-H. Park, S.-W. Oh, S.-T. Myung, Y. C. Kang, and Y.-K. Sun, *Solid State Ionics*, **176**, 481 (2005).
16. S. Jouanneau and J. R. Dahn, *J. Electrochem. Soc*., **151**, A1749 (2004).
17. H.-S. Shin, S.-H. Park, C. S. Yoon, and Y.-K. Sun, *Electrochem. and Solid-State Lett*., **8**, A559 (2005).
18. G.-H. Kim, S.-T. Myung, H. J. Bang, Jai Prakash, and Y.-K. Sun, *Electrochem. and Solid-State Lett*., **7**, A477 (2004).
19. W. Choi and A. Manthiram, *Electrochem. and Solid-State Lett*., **9**, A245 (2006).
20. R. M. Rojas, J. M. Amarilla, L. Pascual, J. M. Rojo, D. Kovacheva, and K. Petrov, *J. Power Sources*, **160**, 529 (2006).
21. B. J. Hwang, R. Santhanam, and S. G. Hu, *J. Power Sources*, **108**, 250 (2002).
22. J.-H. Kim, S.-T. Myung, C. S. Yoon, I.-H. Kang, and Y.-K. Sun, *J. Electrochem. Soc*., **151**, A1911 (2004).
23. J. M. Amailla, *Solid State Ionics*, **127**, 73 (2000).
24. G. Amatucci, Du Pasquier, A. Blyr, T. Zheng, and J.-M. Tarascon, *Electrochim. Acta*, **45**, 255 (2001).